The effective geometry Monte Carlo algorithm: Applications to molecular communication

Fatih Dinc, Leander Thiele, Bayram Cevdet Akdeniz

The Effective Geometry Monte Carlo Algorithm: Applications to Molecular Communication

Fatih Dinc[1,2], Leander Thiele [*2], and Bayram Cevdet Akdeniz[1]

[1] Univ. Lyon, INSA Lyon, INRIA, CITILAB, Lyon, 69100, France
[2]Perimeter Institute for Theoretical Physics, Waterloo, Ontario, N2L 2Y5, Canada

Version: December 17, 2019

Abstract

In this work, we address the systematic biases and random errors stemming from finite step sizes encountered in diffusion simulations. We introduce the Effective Geometry Monte Carlo (EG-MC) simulation algorithm which modifies the geometry of the receiver. We motivate our approach in a 1D toy model and then apply our findings to a spherical absorbing receiver in a 3D unbounded environment. We show that with minimal computational cost the impulse response of this receiver can be precisely simulated using EG-MC. Afterwards, we demonstrate the accuracy of our simulations and give tight constraints on the single free parameter in EG-MC. Finally, we comment on the range of applicability of our results. While we present the EG-MC algorithm for the specific case of molecular diffusion, we believe that analogous methods with effective geometry manipulations can be utilized to approach a variety of problems in other branches of physics such as condensed matter physics and cosmological large scale structure simulations.

1 Introduction

Understanding the communication between complex systems of diffusing molecules requires fast and reliable simulation methods. While many methods have been suggested in the literature to simulate diffusion processes inside such systems, they mainly focus on changing the path of the diffusing molecules to overcome systematic errors that arise from the finite step size. We first give a brief review of these approaches.

Molecular communication is growing in importance [1]. The understanding of communication between nanomachines is extremely important for further development in this area. In this pursuit, molecular communication via diffusion (MCvD) channels has been explored extensively in the literature [2, 3]. Although analytical results are derived for some simple diffusion channels, such as a point transmitter and a spherical absorbing receiver in an unbounded environment [4] and in bounded environments [5, 6], a deeper analysis including more complicated structures requires fast and reliable simulations of sophisticated diffusion channels. To meet this demand, many different simulation frameworks have been proposed in the literature, such as N3Sim [7], NanoNS [8], BiNS2 [9] and AcCoRD [10]. The most simple algorithm performing diffusion channel simulations is usually referred to as a Monte Carlo (MC) simulation algorithm. In this algorithm, the molecules iteratively diffuse inside the channel following a Gaussian probability distribution for their step sizes. In each iteration, the molecule position is calculated and molecules that are inside the volume of the receiver are absorbed [11]. This algorithm performs quite accurately for small step sizes while requiring high computation power, i.e. iteration number, in order to simulate complex systems. For large step sizes, the accuracy of the simulation decreases due a combination of different effects. One such effect, called the intra-step absorption problem, is considered in [10, 12, 13]. This effect arises because some molecules close to the receiver are outside of the receiver boundary at two consecutive iteration steps, whereas in reality some portion of them should have been absorbed in-between these steps. In the literature, different absorption models approximating the behaviour of molecules near the receiver boundary (RMC in [12] and APMC in [13]) are proposed to mitigate the intra-step absorption problem. In general, these methods perform random variable (RV) calculations to accurately describe the absorption probabilities of the molecules while decreasing the required iteration number. RMC requires that the surface of the receiver can be approximated by a flat surface, whereas APMC remains accurate only for large step sizes. Both methods work quite well in their respective regime of applicability at the expense of requiring an additional path-integral-like RV calculation which adds another layer of complexity to the simulation algorithm. However, intra-step absorption is only one of the problems which arise from the finite step size of MC simulations.

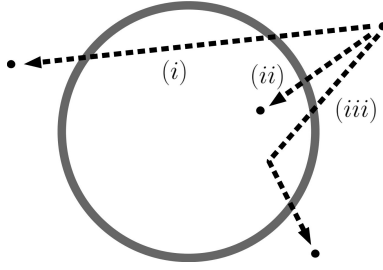*The first two authors contributed equally to this work.

Figure 1: An illustration of various problems resulting from finite step size. (i),(iii): Intra-step absorption problem, (ii): Negative absorption index (NAI) problem
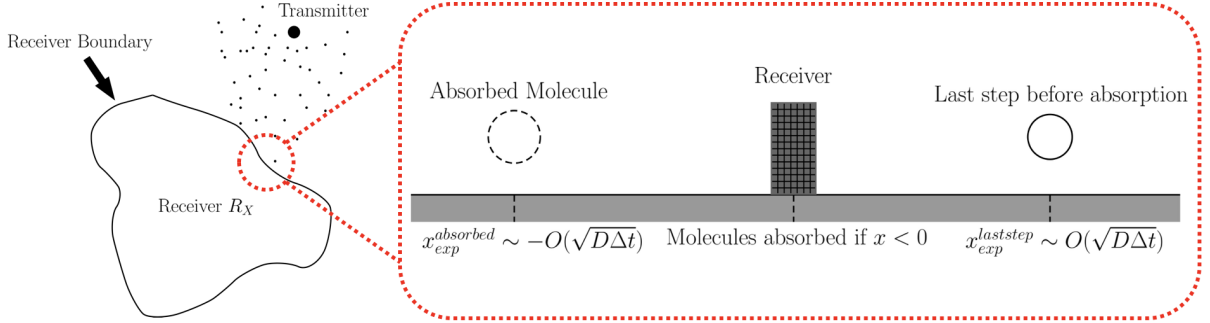

Figure 2: An Illustration of conventional Monte Carlo algorithm for the specific case of 1D. Any smooth surface can be approximated as a 1D as long as the step size is small enough, allowing us to define AI for these surfaces.

In this work, we take a different perspective on the general problem of finite step size. As a first step, we invoke the principle of locality, which asserts that the state of an object can only be affected through its interactions with its nearby surroundings. While being utilized predominantly in physical contexts, such as field theory and relativity, the principle of locality is also pivotal to the Effective Geometry Monte Carlo simulation method (EG-MC) we develop in this article, where we exploit the locality of the absorption of molecules by a receiver. Building up on this intuition, instead of changing the diffusion of molecules near the receiver boundary we introduce an effective absorption surface such that the mean absorption position of the molecules becomes the receiver boundary. By doing so, we both solve the intra-step absorption problem described in the literature [10, 12, 13] and the negative absorption index problem (NAI) which we introduce below. The range of applicability of our method is constrained by the requirement of locality that the step size of the simulation is less than the distance between the receiver and the transmitter.

We organize this paper as follows. We first motivate the negative index problem and introduce the EG-MC algorithm in 1D while showing a way of fixing the free parameter that describes EG-MC. We then apply the EG-MC algorithm to a spherical absorbing receiver described in [4]. Afterwards, we perform an error analysis to show the consistency of our results in different regimes, where we also illustrate the Poisson noise in the simulation. Finally, we conclude with the range of applicability and a quantitative measure of locality in the absorption process.

2 Problem Motivation: 1D Toy Model

We shall consider unbounded diffusion channels of arbitrary dimension first. In d-dimensional diffusion channels, the diffusion process is usually modelled as a Brownian motion with a step size

$$\Delta x_i = \mathcal{N}(0, 2D\Delta t), \quad i = 1, 2, .., d, \tag{1}$$

where D is the diffusion coefficient, Δx_i $(i = 1, 2, .., d)$ are the incremental step sizes in the d-dimensions, Δt is time step, and $\mathcal{N}(\mu, \sigma^2)$ is the normal distribution with mean μ and variance σ^2.

The problems arising from the discrete time steps Δt when diffusing molecules are encountering a boundary are illustrated in Fig. 1. Besides the well-known intra-step absorption problem, we introduce the novel concept of the negative absorption index problem:

Definition (NAI Problem). *We define the absorption index for 1D as*

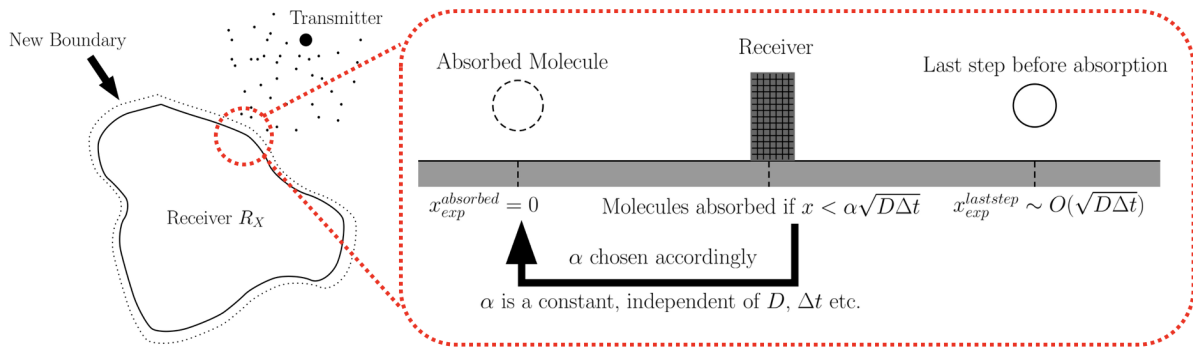$$AI_{1D} = x_{\exp} = \langle x_{\text{absorbed}} - r_x \rangle \tag{2}$$

Figure 3: An Illustration of EG-MC Algorithm both in the general 3D case and in the 1D case. A new boundary is created such that the molecules are absorbed right at the boundary by the algorithm. The main motivation behind the shift of the boundary is the principle of locality, which results in linear relation between the free parameter α and the absorption position x_{exp} (See Fig. 4).

where x_{absorbed} is the absorbed position of the molecule, r_x is the position of the receiver in 1D ($r_x = 0$ unless otherwise stated) and $\langle\rangle$ denotes the average value. Finite step size simulations will always obtain $AI_{1D} < 0$, which we call the negative absorption index (NAI) problem.

Note that this definition of AI is meaningful only in 1D and an analogous definition in higher dimensions requires the surface to be approximately flat on scales comparable to the step size. For the scope of this paper, we deal only with this definition and the results that follow this intuition while leaving a more advanced treatment of the problem as future work.

Consider a conventional MC algorithm, as illustrated in Fig. 2. It is clear that the NAI problem will delay the reception of molecules at the receiver's boundary and therefore deteriorate the simulation's accuracy.

Conversely, a solution of the NAI problem would yield precise results for 1D simulations. This is where the idea of locality becomes significant. If the step size is smaller than the global geometry of the diffusion channel, the absorption process can be considered local. Consequently, an individual molecule's position at distances comparable to the step size from the receiver's boundary can be approximated as independent of the global geometry of the system, hence the local problem has as its only relevant length scale the simulation step size given by $\sqrt{(D\Delta t)}$.

From this it follows immediately that formally shifting the receiver's boundary such that $r_x \rightarrow r_x + \alpha\sqrt{(D\Delta t)}$ as illustrated in Fig. 3 solves the NAI problem if the free parameter α is suitably chosen.

We conclude this section by illustrating the locality property of the receiver. To this aim, we perform simulations of 1D diffusion from a source of molecules[1] situated a distance L from the origin, where the receiver

---

[1] All simulations in this work were performed with 10^5 particles.
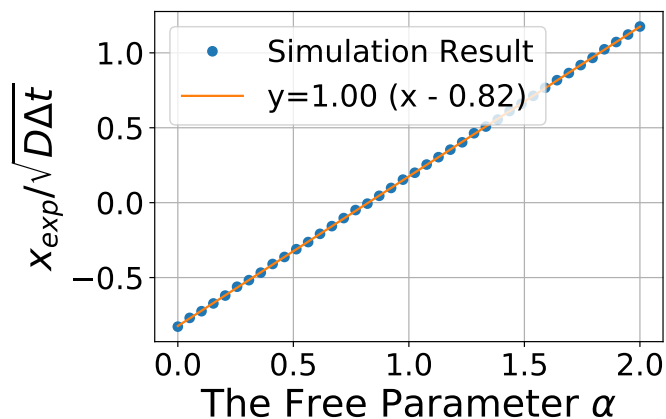
Figure 4: The linear fit describes the relationship between α and x_{exp} (in $1/\sqrt{D\Delta t}$) quite perfectly as expected. For this plot, a range of L ($\in [30, 200]\mu$m) and D ($\in [80, 600]\mu$m^2/s) values are used and the mean values with error bars are plotted. The error bars are much smaller than the marker size. According to multiple trials with different parameters, the most optimum free parameter is $\alpha = 0.8235 \pm 0.0005$. The standard deviation is obtained from the linear fitting performed in this plot.

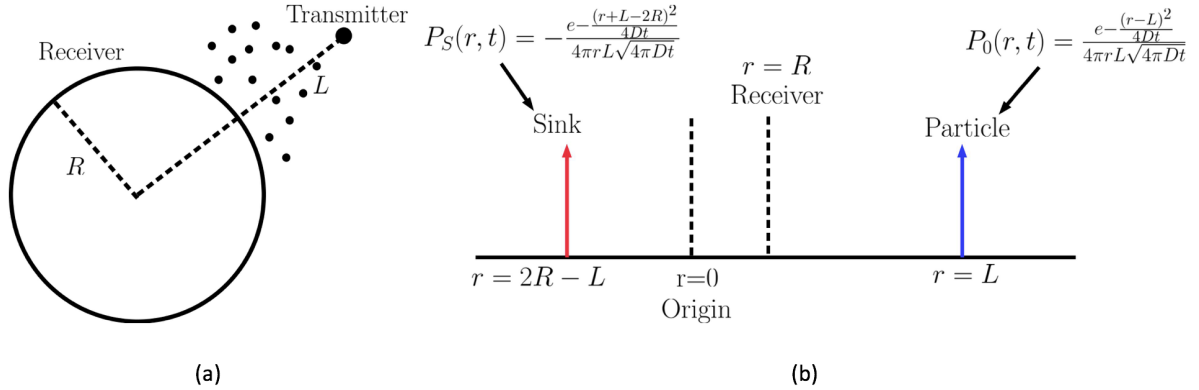Figure 5: (a) The 3D unbounded diffusion channel consisting of a point transmitter and a spherical receiver. (b) The 1D line, where the real space is projected onto the positive values and an imaginary space added to the negative values. In this pseudo-real (consisting of real and extended parts) space, we include a sink at $r = 2R - L$ to use a more general version of method of images.

is located. We use 100 iteration steps. In Fig. 4, $x_{\text{exp}}/\sqrt{(D\Delta t)}$ is plotted against the free parameter α. The shape of this plot is independent of the parameters D and L^2, and the interception of the linear graph with the line $x_{\text{exp}} = 0$ yields the optimum choice for the free parameter $\alpha = 0.8235 \pm 0.0005$ in 1D. In Appendix B we show that an approximate calculation yields a similar value analytically.

3 Application: Spherical Absorbing Receiver

Having motivated the EG-MC algorithm from one-dimensional arguments, we now proceed to apply it to the practically more useful case of a 3D unbounded diffusion channel. As pointed out before, it must be borne in mind that although in 1D the NAI problem was the only systematic bias, in higher dimensions the intra-step absorption problem plays a role as well. We shall show that the EG-MC algorithm still gives results in excellent agreement with the analytic prediction for large step sizes.

We choose our geometry such that a spherical absorbing receiver of radius R is centred at the origin and receives particles from a point source situated a distance L away from the origin, as illustrated in Fig. 5(a).

In order to benchmark our simulation results, we use the analytic expressions available for this problem. They have already been derived in [4] in quite a tedious fashion. We simplify the calculation considerably by introducing the generalized method of images, which we illustrate in Fig. 5(b). The complete derivation is given in Appendix A. It yields for the hitting rate, defined as the particle flux through the boundary

$$n_{\text{hit}}(t) = \frac{R}{L} \frac{L - R}{t\sqrt{4\pi Dt}} \exp\left(-\frac{(R - L)^2}{4Dt}\right), \tag{3}$$

while the fraction of molecules absorbed by the receiver until time t is given by

$$N_{\text{tot}}(t) = \int_0^t n_{\text{hit}}(\tau) \, \mathrm{d}\tau = \frac{R}{L}\text{erfc}\left[\frac{L - R}{\sqrt{4Dt}}\right]. \tag{4}$$

We now proceed by applying the EG-MC algorithm (Algorithm 1) to the 3D diffusion channel described above. The algorithm has the same structure as the Monte Carlo simulations, with the exception of line 7. Here, unlike usual Monte Carlo algorithms, we add a small thickness to the spherical receiver using the intuition we derived from the 1D toy model in the previous section. From now on, we denote the Monte Carlo simulations as the $\alpha = 0$ limit of our algorithm. Moreover, as $\Delta t \to 0$, our algorithm converges to the Monte Carlo algorithm, as expected.

For this section, we pick $\alpha = 0.8235$ for illustrative purposes (and shall explore the constraints on the parameter in Sec. 4). A comparison between simulation and analytical results is given in Figs. 6 and 7. As can be seen from the figures, EG-MC outperforms the Monte Carlo algorithm significantly. Moreover, our algorithm gives robust results for far larger step sizes, hence decreasing the computational cost extremely. For example, in Fig. 7, the EG-MC algorithm converges in less than 300 iterations (we find that 20-30 iterations are the empirical cut-off for these cases where EG-MC performs quite well) while the Monte Carlo algorithm does not converge even for 10000 iterations.

---

[2]This has been found to hold for $D \in [80, 600]\mu\text{m}^2/\text{s}$ and $L \in [30, 200]\mu\text{m}$.
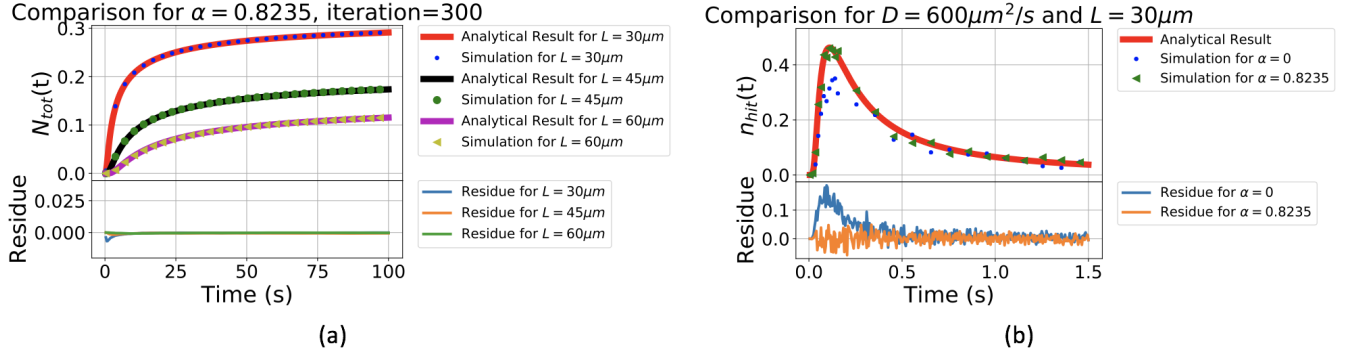
Figure 6: (a) The proof of concept that EG-MC algorithm produces correct results for various transmitter distance L, where $D = 80\,\mu\mathrm{m}^2/\mathrm{s}$ and $R = 10\mu\mathrm{m}$. (b) The comparison of $n_{\mathrm{hit}}(t)$ obtained from both simulations with the analytical result. As can be seen, the EG-MC algorithm produces a result which follows the analytical curve closely. For both cases, the iteration number is taken as 300 and the step size can be calculated as $\Delta t = t_f/\mathrm{iteration}$, where t_f is the final time of the simulation.
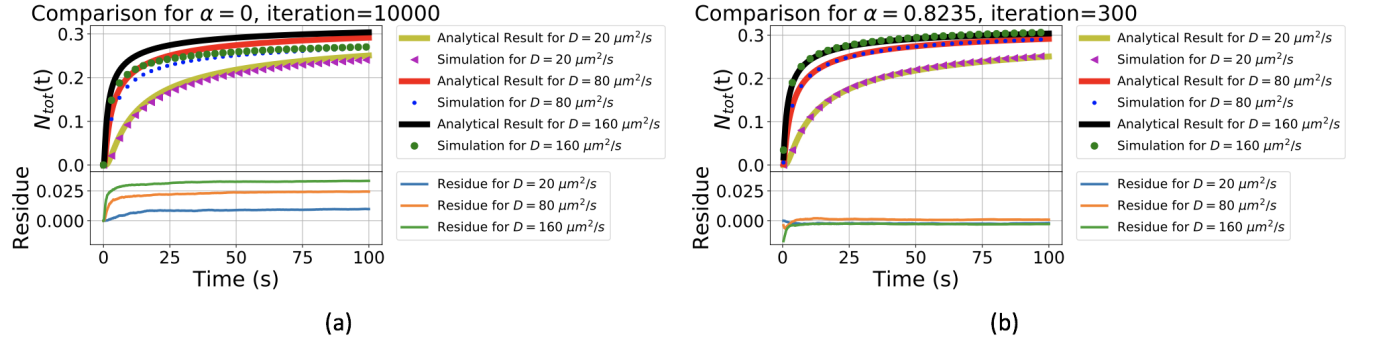

Figure 7: The comparison of Monte Carlo simulation (a) and EG-MC simulation (b) with the analytical solution for different D values, where $L = 30\,\mu\mathrm{m}$ and $R = 10\mu\mathrm{m}$. For each individual case, the step size is different and therefore we note the value of total iteration. The step size can be calculated as $\Delta t = t_f/\mathrm{iteration}$, where t_f is the final time of the simulation.

Algorithm 1 Effective Geometry Monte Carlo (EG-MC)

1: **procedure** ABSORPTION DETECTION(x_i for i=1,2,3)
2:     Define iteration number, initial position and simulation parameters $(D,L,\Delta t)$
3:     $t_f = \Delta t \cdot \mathrm{iteration}$
4:     **for** i = 1:iteration **do**
5:         Perform Diffusion Simulation
6:         $r = \sqrt{x^2 + y^2 + z^2}$
7:         index=find($r < r_x + \alpha\sqrt{D\Delta t}$)
8:         $N_{\mathrm{abs}}(i)=$ length(index)
9:         (x,y,z)[index]=[]   ▷ Molecules are absorbed
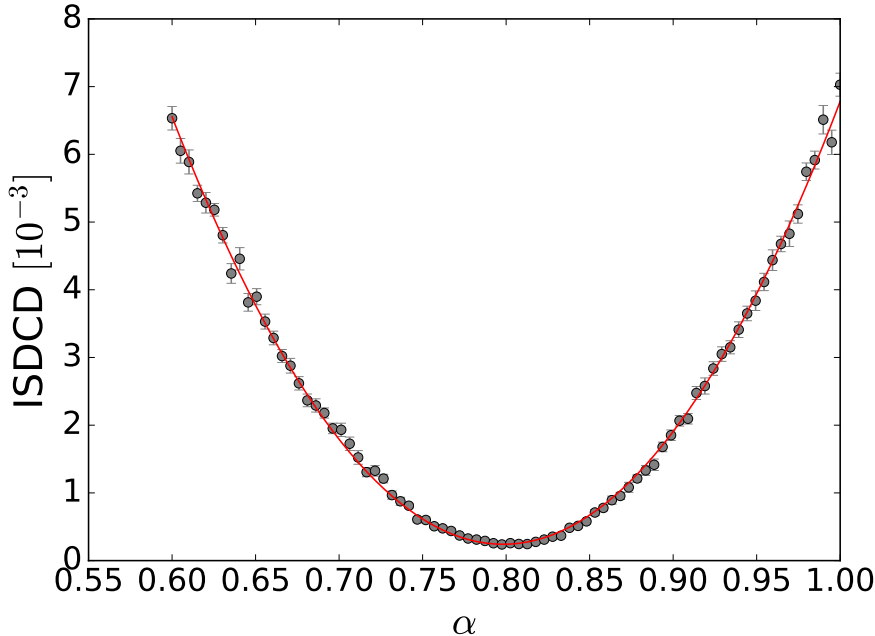10:   **end for**
11:     **return** N_{abs}

Figure 8: Dependence of ISDCD as defined in Eq. (6) on α for $L = 35\,\mu$m, $R = 10\,\mu m$, $D = 80\,\mu\text{m}^2/\text{s}$. The simulation was run with 100 iterations for each choice of α. Errorbars were obtained by running the simulation 20 times for each α and taking $\sigma_{\text{ISDCD}} = \sqrt{(\text{Var}(\text{ISDCD})/20)}$. The fit is a simple parabola.

Before moving on to the error analysis, we shall first define some short-hand notations. From now on, we denote the discretized values by a square bracket, e.g. $N[\cdot]$. Furthermore, we denote the number of particles absorbed between times t_i and $t_i + \Delta t$ as

$$\Delta N_{\text{tot}}[t_i] = N_p \int_{t_i}^{t_i+\Delta t} n_{\text{hit}}(\tau)\,\mathrm{d}\tau. \tag{5}$$

Here, N_p denotes the number of particles initially released by the transmitter.

4 Error and Efficiency Analysis

In this section we discuss the uncertainty on the parameter α introduced above. To this aim, we compare the simulation result for a given α with the analytic result.

First, we define the integrated squared difference in the cumulative distribution (ISDCD) as

$$\text{ISDCD} = \sum_i (N_{\text{tot}}^{\text{sim}}[t_i] - N_{\text{tot}}^{\text{anl}}[t_i])^2, \tag{6}$$

where the sum runs over all data points in a given simulation, and "sim" and "anl" denote the simulated and analytical results respectively. We choose this quantity as our primary measure for the accuracy of a given simulation for the following reasons: The cumulative distribution is a better measure than the bare probability density function (hit rate), since it mitigates the random noise in the simulation. Instead of comparing the cumulative distribution at a certain point in time, we use the sum, because it is less susceptible to random fluctuations, which are of particular importance in the steep increase of the cumulative distribution for small times.

In Fig. 8 we show the dependence of the ISDCD on the choice of the parameter α. It can clearly be seen that the ISDCD has a well defined minimum around $\alpha \sim 0.8$, and follows a quadratic dependence as confirmed by the fit.

Utilizing this behaviour, we can estimate the optimum value of α for different choices of simulation parameters (R, L, D) and different iteration numbers. This is easily done by retrieving the ISDCD, fitting it with a parabola and retrieving the value α that minimizes the ISDCD. A measure for the error on α is obtained by repeating this procedure (20 times) and taking the standard deviation of the results.

It may be argued that the better known reduced chi-squared χ^2_{red} of the simulated hitting rate with respect to the analytic hitting rate is a better estimator for the goodness of the simulation, since it directly describes the simulated data. However, as argued before, this quantity is very susceptible to random fluctuations. Nonetheless, we demonstrate that the optimal choice of α from the ISDCD corresponds to expected values of χ^2_{red}. We define

$$\chi^2_{\text{red}} = \frac{1}{\text{iteration} - 1} \sum_i \left(\frac{\Delta N_{\text{tot}}^{\text{sim}}[t_i] - \Delta N_{\text{tot}}^{\text{anl}}[t_i]}{\sigma[t_i]} \right)^2, \tag{7}$$
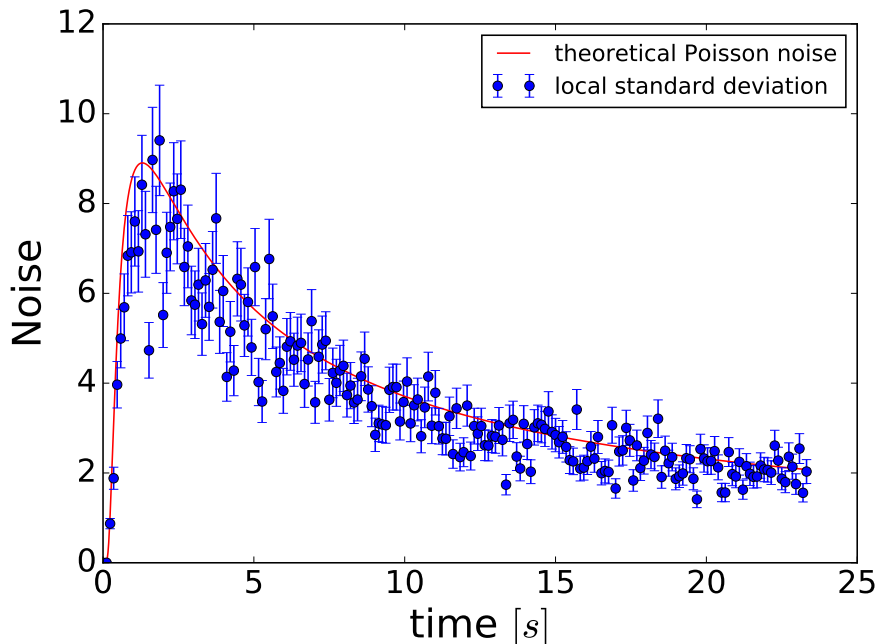
6

Figure 9: Standard deviation of the hitting rate taken from 30 simulations in dependence on time. The simulations were performed with $L = 35\,\mu$m, $R = 10\,\mu$m, $D = 80\,\mu$m^2/s, $N = 10^3$ iterations. We computed the error bars approximating the hitting rate as normally distributed.[4] The red line is the theoretical expectation for Poisson noise $\sqrt{(\Delta N_{\text{tot}}^{\text{anl}}[t_i])}$. For clarity, only every fifth datapoint is shown.

where we take ΔN_{tot} as the bare count rate in our simulation (i.e. it is integer valued and not normalized as in the previous sections).

We expect the random error $\sigma[t_i]$ to be close to Poisson noise.[3] We confirm this by running the simulation repeatedly, retrieving for each datapoint the difference to the analytic result, and taking the standard deviation. The result is shown in Fig. 9, and confirms that we can set $\sigma^2[t_i] = \Delta N_{\text{tot}}^{\text{anl}}[t_i]$. This is in agreement with the various models proposed in the literature [14, 15].

In Fig. 10 we show the results for the optimum value of α as estimated from the ISDCD, together with the corresponding χ_{red}^2 values from $\Delta N_{\text{tot}}[t_i]$.

We first discuss the behaviour of the optimal parameter α_O for different simulation inputs. It is clear that α_O varies only very slightly, although the simulations were performed with very different input parameters. This confirms our expectation that to a good approximation we can treat α_O as a constant. However, the deviations from the weighted mean are larger than expected from the errorbars. This is mainly due to a systematic effect at low iteration numbers, as for those the local problem at the receiver's boundary begins to loose its one-dimensional character which we invoked to motivate the EG-MC method. In general, we find the optimum α to be slightly lower in the 3D case in comparison to the 1D case, which we attribute to the fact that the α-correction increases the total number of particles received integrated over all time (according to R/L), while in 1D all particles are absorbed.

Next we discuss the behavior of χ_{red}^2. It is well known that an optimal fit is characterized by $\chi_{\text{red}}^2 = 1$, and it can be seen that this value is obtained – within statistical errors – for each simulation shown. We also list the values of χ_{red}^2 for identical simulation parameters if α is set to 0. It is clear from these values that the EG-MC method outperforms a naive implementation by a large margin for iteration numbers of order 10^2, while for larger iteration numbers the chi-squared is not a good measure for the goodness of fit due to the large standard deviation stemming from the Poisson noise.

After showing that the EG-MC method results in a better fit than the MC algorithm, we can now focus on comparing both algorithms in terms of efficiency. Before starting the comparison, we emphasize once more that the implementation of EG-MC algorithm is identical to the MC algorithm, with the only difference being the non-zero free parameter α in Algorithm 1. For the rest of this section, we will perform chi-squared and relative error analyses to assess the correctness of the simulations, which are performed with increasing iteration number. As a first order approximation, the simulation time linearly increases with the iteration number of the simulation. 10^5 particles are released from the transmitter for each simulation, whereas the time interval of the simulations is taken as $t \in [0, t_{\text{ch}}]$. Here, we define the characteristic time scale for each scenario as

$$t_{\text{ch}} = \frac{(R-L)^2}{D}. \tag{8}$$

This definition is particularly important for comparison of different scenarios, as the time-scale should be

---

[3]There is a small correction due to correlations between different time steps, as a high absorption rate in one time step in general leads to a lower absorption rate in the consecutive step. However, this effect is found to be very small.

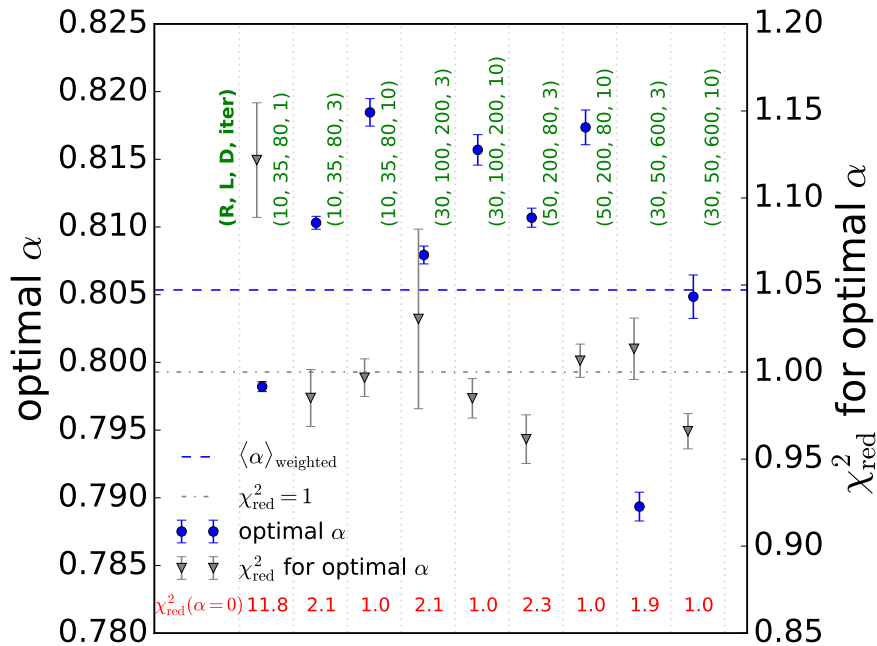[4]According to the formula $\text{Var}(\sigma) = \sigma^2\{1 - 2\Gamma^2(N/2)/[(N-1)\Gamma^2((N-1)/2)]\}$.

Figure 10: Blue datapoints are the optimal value of α for different input parameters, estimated from the IS-DCD as described in the text. The grey triangles indicate the value of χ^2_{red} obtained with this choice of α. We also list the values of χ^2_{red} for a simulation in which $\alpha = 0$ at the bottom of the plot. The average $\langle \alpha \rangle$ is weighted with the square of the individual standard deviations. The values (R, L, D, iter) are given in units of $(\mu\mathrm{m}, \mu\mathrm{m}, \mu\mathrm{m}^2/\mathrm{s}, 10^2)$.

equivalent in all cases. We note that t_{ch} corresponds to $6\tau_{\mathrm{peak}}$, where τ_{peak} is the time $n_{\mathrm{hit}}(t)$ reaches its maximum [4]. Therefore, the simulations are space and time scale-invariant for the time interval $[0, t_{\mathrm{ch}}]$.

We compare the results of the chi-squared analysis for both algorithms with increasing iteration number in Fig. 11. Chi-squared analysis gives us the minimum iteration number after which the systematic error per time slot caused by the algorithm is less than the random error. Due to the scale invariance of the simulations, the χ^2_{red} values follow the same pattern with increasing iteration number (hence lower step size) as expected. The accuracy of the algorithm depends on the only scale-free parameter, which is the step-size adjusted with respect to the channel parameters (hence the iteration number). As can be seen from the figures, the iteration number required by MC algorithm to have similar accuracy as the EG-MC algorithm is around 1000. This shows that for the systematic error per time slot to be smaller than the random error, MC algorithm requires an order of magnitude larger simulation time with respect to the EGMC algorithm. While systematic error per time slot might be smaller than the random error, the algorithm can still make incorrect predictions for metrics where random error is integrated out. This is particularly clear from $N_{\mathrm{tot}}(t)$ plotted in each subfigure, as the MC algorithm still cannot predict the correct values. The reason is as following: While the systematic error in $n_{\mathrm{hit}}(t)$ is smaller than the random error, integrating out the random error to obtain $N_{\mathrm{tot}}(t)$ accumulates the systematic error, resulting in the inaccurate prediction. However, the expected fraction of particles absorbed by the receiver is an important channel parameter which should be predicted accurately.

In order to test the algorithms in terms of their prediction of parameters where random errors are integrated out and systematic errors are accumulated, we propose the following metric, called the relative error:

$$\varepsilon_{\mathrm{rel}} = \frac{1}{\mathrm{iteration}} \sum_{t=\Delta t}^{t_{max}} \frac{|N^A_{\mathrm{tot}}(t) - N^S_{\mathrm{tot}}(t)|}{N^A_{\mathrm{tot}}(t)}. \tag{9}$$

Here, S/A stands for simulation/analytic result. In implementing this metric, we occasionally use an offset, starting the sum from offset $\times \Delta t$ instead of Δt and adjusting the divison factor, as for the early times the random error still dominates for this metric. The result of the relative error analysis is shown in Fig. 12. As can be seen from the figure, the MC algorithm matches the accuracy of the EGMC algorithm around 30000 iterations, whereas the EGMC algorithm makes accurate predictions even for 300 iterations. This shows that the EGMC algorithm requires 2 orders of magnitude less iteration to converge to the analytic result. As to the first order approximation, simulation time linearly scales with the iteration number, the EGMC algorithm outperforms the MC algorithm while being more efficient in terms of simulation time by 2 orders of magnitude.

5 Range of Applicability and Application to Complex Structures

The last topic we shall address is the range of applicability of the EG-MC algorithm. As we have already discussed, the principle of locality dictates that $\sqrt{(2D\Delta t)} \ll O(L)$. In other words, the step size should be
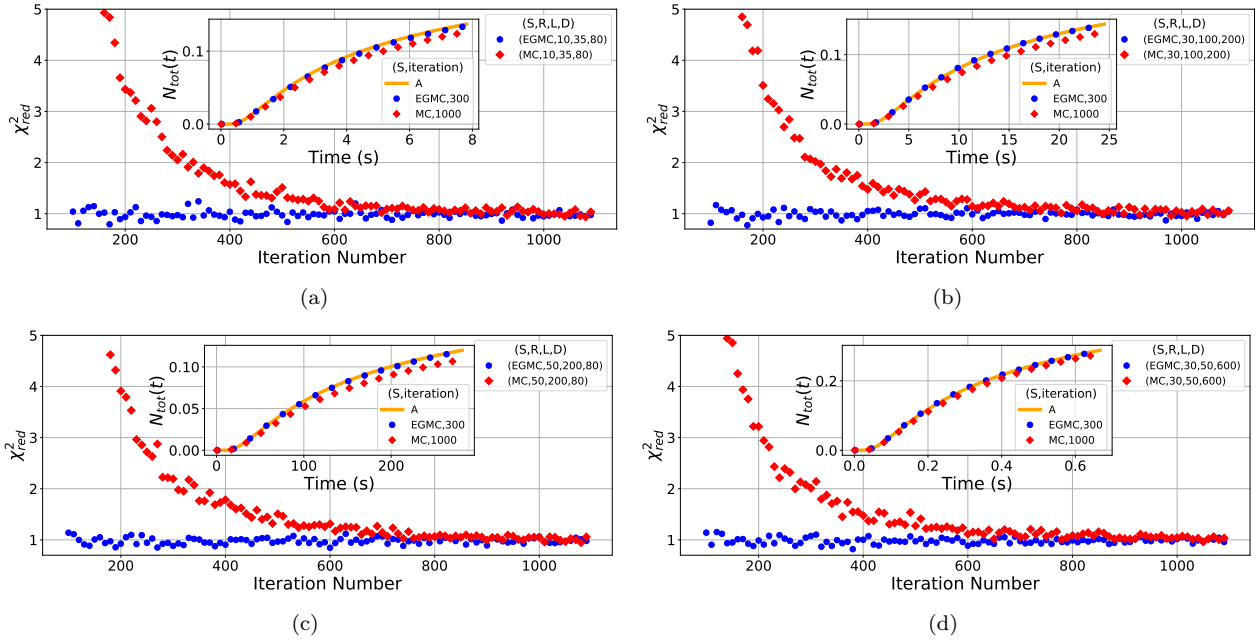
Figure 11: The reduced chi-squared analysis to test the accuracy of the EGMC and MC algorithm. The final time is t_{ch} for all cases and the simulation time step can be found by $\Delta t = t_{\mathrm{ch}}/\mathrm{iteration}$.
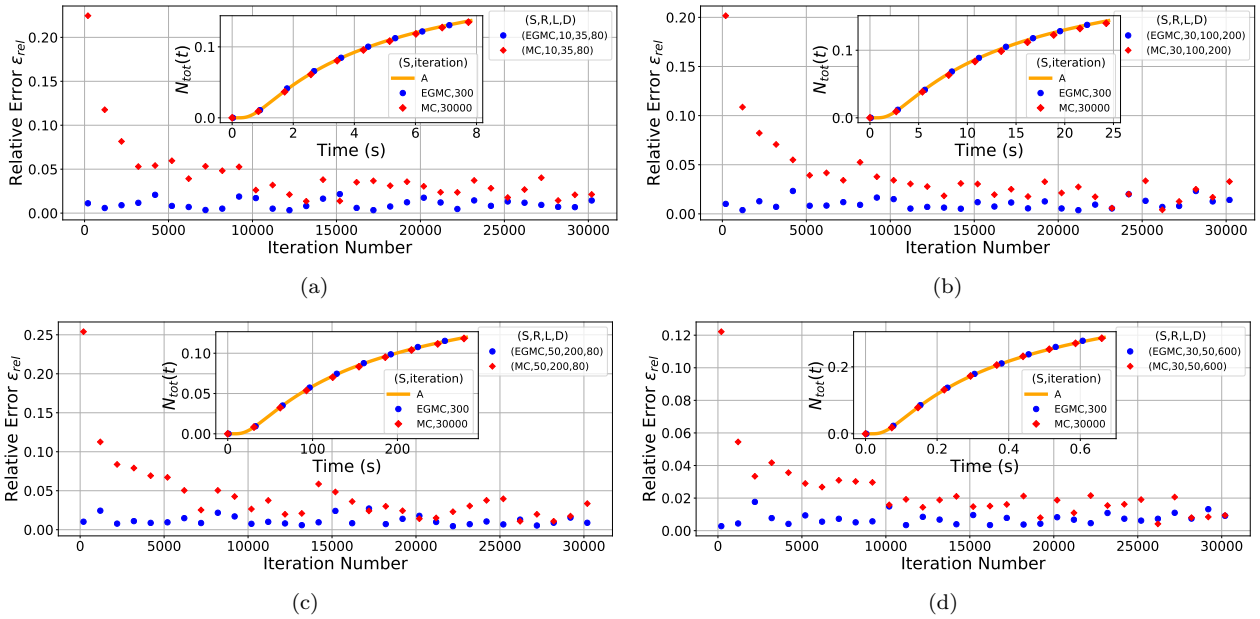

Figure 12: The relative error analysis to test the accuracy of the EGMC and MC algorithm. The final time is t_{ch} for all cases and the simulation time step can be found by $\Delta t = t_{\mathrm{ch}}/\mathrm{iteration}$.
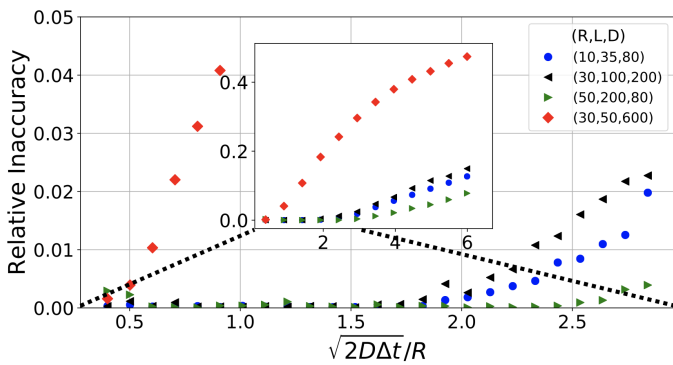
Figure 13: The relative inaccuracy between the Monte Carlo simulations and the EG-MC simulations for various step sizes. The iteration number is chosen such that either the final time is $6\times$ the peak value of $n_{\mathrm{hit}}(t)$ or at least 100 iterations to allow more accurate comparison between different cases. EG-MC algorithm clearly outperforms MC simulations for various step sizes. More importantly, EG-MC algorithm results in negligible error as long as $\sqrt{(2D\Delta t)} \leq L - R$, i.e. the locality assumption is valid.

9

small enough such that the molecules are not absorbed after only a few steps. To illustrate this concept, we define a comparison metric called relative inaccuracy as follows

$$\text{Relative inaccuracy} = \frac{\text{ISDCD}(\alpha = 0.8235)}{\text{ISDCD}(\alpha = 0)}. \tag{10}$$

Here ISDCD(α) is the integrated squared difference in the cumulative distribution defined in Eq. (6), which we evaluate for the EG-MC algorithm and compare it with a simple Monte Carlo implementation. In Fig. 13, we show the relative inaccuracy in dependence on step size for various choices of (R, L, D). It shows that our algorithm performs very well even for step sizes larger than the diameter of the receiver provided that a cutoff value related to the locality condition is not exceeded. In our calculations, we find that the cutoff condition can be given more precisely as

$$\sqrt{2D\Delta t} \lesssim L - R. \tag{11}$$

We can clearly see in Fig. 13 that this cutoff value is observed for the four different cases we present in this paper.

So far, we have focused on the case with a spherical absorbing receiver and a point transmitter. Now, we shall generalize our findings to more general systems with multiple transmitters and receivers having arbitrary shapes. We will start by showing that the EGMC algorithm converges to the MC algorithm for the time steps Δt, for which MC algorithm is reliable. Let us re-consider Figs. 11 and 12. The time step in these simulations can be given as

$$\Delta t = \frac{t_{\text{ch}}}{\text{iteration}} = \frac{(R - L)^2}{D \times \text{iteration}}. \tag{12}$$

The incremental increase in the spherical receiver radius can be given as $\alpha\sqrt{D\Delta t} = \alpha(R-L)/\sqrt{\text{iteration}}$. Then, we can find the fractional increase, ΔR, in the receiver radius as

$$\Delta R = \alpha\frac{R - L}{R\sqrt{\text{iteration}}} \sim 10^{-2}, \tag{13}$$

where we realize that $\alpha\frac{R-L}{R} \sim O(1)$ and iteration $\sim O(10^4)$ for the case where MC algorithm performs accurately. In the regime where MC algorithm is reliable, EGMC algorithm requires a single percent increase in the spherical radius, which can easily be neglected. This shows that as a lower bound, the EGMC algorithm performs as good as the MC algorithm in any complex structure.

Then, we argue using locality principle that the EGMC algorithm retains its superiority to the MC algorithm for a large group of complex structures. Let us assume that there are many receivers inside a channel. For the EGMC algorithm to be accurate, we require that the position step size, $\sqrt{2D\Delta t}$, in each iteration should be smaller than the distance smallest distance between the receivers. If this requirement is satisfied, changing the radius of one receiver does not affect the diffusion of molecules close to the other receivers[5], while correcting the systematic error caused by the MC algorithm around the original receiver. Since locality condition given in (11) is less strict than the high iteration number condition of the MC algorithm, the EGMC algorithm is expected to outperform MC algorithm in any complex structure. This shows that using the EGMC algorithm is always preferred over using MC algorithm.

Finally, we conclude with specific examples where hte EGMC algorithm has been tested. In [16], the EGMC algorithm is applied for spherical absorbing receivers in an n-dimensional diffusion channel. Furthermore, in [Accepted article, in production], it is shown that MC algorithm leads to a systematic shift in the absorption angle of molecules. The EGMC algorithm fixes this problem, which shows that the EGMC algorithm truly solves the intra-step absorption problem[6]. Moreover, in this work, it is shown that the EGMC algorithm works accurately in the presence of constant flow as well, laying evidence for our claim that the EGMC algorithm can perform accurately in complex channels.

6 Conclusion

In this paper, we have shown that an effective geometry approach can lead to significantly faster and more reliable simulations of diffusion in molecular communication. As the complete method solely consists of including a small correction – $\alpha\sqrt{(D\Delta t)}$ – to the receiver radius, it decreases the computational cost significantly. In fact, we have shown, in Fig. 7, that while EG-MC converges for iteration numbers ~ 300, the Monte Carlo simulation does not converge to the analytical solution even for ~ 10000 in the case of a spherical receiver.

---

[5]By this, we mean that the interference probability between the two receivers is suppressed by a Gaussian according to the distance between them and the time step Δt.

[6]This is because the EGMC algorithm predicts both the hitting rate and the absorption angle accurately, meaning that it mimics the diffusion process completely.

From this perspective, our method outperforms Monte Carlo simulations by more than two orders of magnitude in terms of computation time.

We also note that the possibility of choosing a relatively large step size mitigates the problem of Poisson noise considerably, which implies that the simulation can be run with a smaller number of particles if identical noise levels for the hitting rate are to be obtained.

We believe that the EG-MC algorithm we present in this paper is just a first step towards a deeper understanding of effective geometries in the optimization of Monte Carlo type simulations. Similar algorithms can be implemented in different fields using Monte Carlo simulations where computational cost is of primary importance. As future work, we plan to generalize our findings to higher dimensional spaces while applying EG-MC algorithm for complex systems consisting of multiple receivers/transmitters with arbitrary shapes. Through the computational efficiency this method introduces, many systems deemed too complex to be simulated in reasonable time intervals should be considered for further research directions.

Acknowledgements

References

[1] N. Farsad, H. B. Yilmaz, A. Eckford, C.-B. Chae, and W. Guo, "A comprehensive survey of recent advancements in molecular communication," *IEEE Communications Surveys & Tutorials*, vol. 18, no. 3, pp. 1887–1919, 2016.

[2] H. B. Yilmaz and C.-B. Chae, "Arrival modelling for molecular communication via diffusion," *Electronics Letters*, vol. 50, no. 23, pp. 1667–1669, 2014.

[3] T. Nakano, Y. Okaie, and J.-Q. Liu, "Channel model and capacity analysis of molecular communication with brownian motion," *IEEE communications letters*, vol. 16, no. 6, pp. 797–800, 2012.

[4] H. B. Yilmaz, A. C. Heren, T. Tugcu, and C.-B. Chae, "Three-dimensional channel characteristics for molecular communications with an absorbing receiver," *IEEE Communications Letters*, vol. 18, no. 6, pp. 929–932, 2014.

[5] F. Dinc, B. C. Akdeniz, A. E. Pusane, and T. Tugcu, "Impulse response of the channel with a spherical absorbing receiver and a spherical reflecting boundary," *CoRR*, vol. abs/1804.03383, 2018. [Online]. Available: http://arxiv.org/abs/1804.03383

[6] M. M. Al-Zubi and A. S. Mohan, "Modeling of ligand-receptor protein interaction in biodegradable spherical bounded biological micro-environments," *IEEE Access*, vol. 6, pp. 25 007–25 018, 2018.

[7] I. Llatser, D. Demiray, A. Cabellos-Aparicio, D. T. Altilar, and E. Alarcón, "N3sim: Simulation framework for diffusion-based molecular communication nanonetworks," *Simulation Modelling Practice and Theory*, vol. 42, pp. 210–222, 2014.

[8] E. Gul, B. Atakan, and O. B. Akan, "Nanons: A nanoscale network simulator framework for molecular communications," *Nano Communication Networks*, vol. 1, no. 2, pp. 138–156, 2010.

[9] L. Felicetti, M. Femminella, G. Reali, P. Gresele, and M. Malvestiti, "Simulating an in vitro experiment on nanoscale communications by using bins2," *Nano Communication Networks*, vol. 4, no. 4, pp. 172–180, 2013.

[10] A. Noel, K. C. Cheung, R. Schober, D. Makrakis, and A. Hafid, "Simulating with accord: Actor-based communication via reaction–diffusion," *Nano Communication Networks*, vol. 11, pp. 44–75, 2017.

[11] H. B. Yilmaz and C.-B. Chae, "Simulation study of molecular communication systems with an absorbing receiver: Modulation and isi mitigation techniques," *Simulation Modelling Practice and Theory*, vol. 49, pp. 136–150, 2014.

[12] D. Arifler and D. Arifler, "Monte carlo analysis of molecule absorption probabilities in diffusion-based nanoscale communication systems with multiple receivers," *IEEE transactions on nanobioscience*, vol. 16, no. 3, pp. 157–165, 2017.

[13] Y. Wang, A. Noel, and N. Yang, "A novel a priori simulation algorithm for absorbing receivers in diffusion-based molecular communication systems," *arXiv preprint arXiv:1809.00808*, 2018.

[14] H. Arjmandi, A. Gohari, M. N. Kenari, and F. Bateni, "Diffusion-based nanonetworking: A new modulation technique and performance analysis," *IEEE Communications Letters*, vol. 17, no. 4, pp. 645–648, 2013.

[15] A. Etemadi, P. Azmi, H. Arjmandi, and N. Mokari, "Compound poisson noise sources in diffusion-based molecular communication," 2018.

[16] F. Dinc, "Analytical estimation for the impulse response of an n-dimensional diffusion channel with an absorbing receiver," *Journal of Physics A: Mathematical and Theoretical*, vol. 52, no. 11, p. 11LT01, 2019.

A   Derivation of the Hitting Rate via Generalized Method of Images

In this appendix, we derive the analytic expression for the hitting rate $n_{\text{hit}}(t)$ and the integrated fraction of particles absorbed $N_{\text{tot}}(t)$ in the geometry described in Sec. 3.

The impulse response for this diffusion channel has already been derived in [4]. Here, we shall re-derive their findings while motivating the solution by symmetry arguments rather than lengthy calculations.

The diffusion of molecules in 3D is described by Fick's Law

$$\boldsymbol{\nabla}^2 P(r,t) = D\partial_t P(r,t) \tag{14}$$

where $\boldsymbol{\nabla}^2$ is the Laplacian operator, $P(r,t)$ is the probability distribution function of a diffusing molecule, D the diffusion coefficient defined in Eq. (1) and ∂_t is the partial derivative with respect to t.

The receiver absorbs all the molecules upon incident. Moreover, the molecules are initially localized at the position $(0,0,L)$. These two conditions specify a unique solution for the diffusion equation. Nonetheless, before proceeding, we shall exploit the SO(3) symmetry. The absorption angle of the molecules is dependent on the initial position of the transmitter, whereas the absorption rate is not. As we are only interested in the absorption rate, we can solve an equivalent but easier initial value problem in which the transmitter position is symmetrised over all angles. Then, the boundary conditions become

$$P(r,0) = \frac{\delta(r-L)}{4\pi r^2}, \tag{15a}$$

$$P(R,t) = 0. \tag{15b}$$

The calculation presented in [4] derives its substantial length from the boundary condition in Eq. (15b). To avoid this, let us first write down the solution to the diffusion equation subject only to Eq. (15a), which is describing a freely diffusing particle [4]

$$P_0(r,t) = \frac{\exp\left(-\frac{(r-L)^2}{4Dt}\right)}{4\pi r L \sqrt{4\pi Dt}}. \tag{16}$$

One important realization regarding this solution is that L is a free parameter, i.e. the diffusion equation is satisfied regardless of its choice, while L ensures that the boundary condition Eq. (15a) holds.

As the system is symmetric around all angles, we can project it onto a line stretching from 0 to ∞. This transformation maps $4\pi r'^2\,\mathrm{d}r'$ points onto $\mathrm{d}r$ points where $r \in [0,\infty)$ is the parameter describing the real line. Usually this transformation is irreversible as it is not one-to-one. Nonetheless, by the SO(3) symmetry, no information is lost during the transformation. With this in mind, we can project the complete 3D space into an incomplete 1D real space $r \in [0,\infty)$ with $r = 0$ describing the origin of the original space. Then, we complete this space by adding the negative values for r, as shown in Fig. 5(b), which do not have any physical meaning for the 3D space but are useful in solving the diffusion equation. As a final step, we include a sink at $r = 2R - L$ with

$$P_S(r,t) = -\frac{\exp\left(-\frac{(r+L-2R)^2}{4Dt}\right)}{4\pi r L \sqrt{4\pi Dt}}, \tag{17}$$

while recalling that the diffusion space is $r \geq R$. From the uniqueness theorem it follows that $P(r,t) = P_0(r,t) + P_S(r,t)$ is the desired solution, as it satisfies the boundary conditions and the diffusion equation. Now, we can transform back to 3D space, where both $P_S(r,t)$ and $P_0(r,t)$ remain invariant due to the SO(3)

symmetry. This symmetry-motivated method is a more general version of the method of images which is used commonly in the literature. Hence, we obtain the probability distribution function for the molecule as

$$P(r,t) = \frac{\exp\left(-\frac{(r-L)^2}{4Dt}\right) - \exp\left(-\frac{(r+L-2R)^2}{4Dt}\right)}{4\pi r L \sqrt{4\pi Dt}}. \tag{18}$$

Then the hitting rate, defined as the particle flux through the boundary, is given by

$$n_{\text{hit}}(t) = 4\pi R^2 D\, \partial_r P(r,t)|_{r=R} = \frac{R}{L}\frac{L-R}{t\sqrt{4\pi Dt}}\exp\left(-\frac{(R-L)^2}{4Dt}\right). \tag{19}$$

The fraction of molecules absorbed by the receiver until time t follows as

$$N_{\text{tot}}(t) = \int_0^t n_{\text{hit}}(\tau)\,\mathrm{d}\tau = \frac{R}{L}\mathrm{erfc}\left[\frac{L-R}{\sqrt{4Dt}}\right]. \tag{20}$$

B Analytical Approximation for α

In this appendix, we are deriving an approximate expression for α in the 1D case. We choose our geometry such that the receiver is located at $x = 0$, and the effective receiver at α'. Let us consider a single time step in the simulation. At the beginning of the step, a particle is located at $x_0 > \alpha'$. We first find the expected absorption position $\langle x_1(x_0)\rangle$ for this individual particle under the assumption that it is absorbed. We choose our units of length such that the probability density function for the location of this particle after the time step is given by

$$P(x,x_0) = N\mathrm{e}^{-(x-x_0)^2}, \tag{21}$$

where we omit normalization factors and lump them in N because they are of no importance for the calculation and would only serve to clutter the expressions.

Hence we find that

$$\langle x_1(x_0)\rangle = \frac{\int_{-\infty}^{\alpha'}\mathrm{d}x\, x P(x,x_0)}{\int_{-\infty}^{\alpha'}\mathrm{d}x\, P(x,x_0)}. \tag{22}$$

The probability of absorption is given by

$$P_{\text{abs}}(x_0) = \int_{-\infty}^{\alpha'}\mathrm{d}x\, P(x,x_0). \tag{23}$$

Denoting the instantaneous distribution of particles by $\rho(x_0)$, the expected absorption position can then be given by using the probability distribution $(P_{\text{abs}}(x_0)\rho(x_0)\,\mathrm{d}x_0)$ as

$$\langle x_{\text{abs}}\rangle = \frac{\int_{\alpha'}^{\infty}\mathrm{d}x_0\, \langle x_1(x_0)\rangle P_{\text{abs}}(x_0)\rho(x_0)}{\int_{\alpha'}^{\infty}\mathrm{d}x_0\, P_{\text{abs}}(x_0)\rho(x_0)}, \tag{24}$$

We now want to find α' such that the expected absorption position (for all particles present at $x > \alpha'$) equals zero. It follows that

$$0 = \int_{\alpha'}^{\infty}\mathrm{d}x_0\, \langle x_1(x_0)\rangle P_{\text{abs}}(x_0)\rho(x_0), \tag{25}$$

We now invoke the approximation that the distribution $\rho(x_0)$ is uniform. This approximation will yield a relatively precise result for α because only particles relatively close to the receiver have an appreciable chance of absorption, which justifies a zeroth order approximation.

Inserting the expressions given before, we find

$$0 = \int_{\alpha'}^{\infty}\mathrm{d}x_0\int_{-\infty}^{\alpha'}\mathrm{d}x\, x\mathrm{e}^{-(x-x_0)^2}. \tag{26}$$

Performing the change of variables $\chi \equiv x - x_0$ in the second integral, we find

$$0 = \int_{\alpha'}^{\infty}\mathrm{d}x_0\int_{-\infty}^{\alpha'-x_0}\mathrm{d}\chi\left(\chi\mathrm{e}^{-\chi^2} + x_0\mathrm{e}^{-\chi^2}\right) = \int_{\alpha'}^{\infty}\mathrm{d}x_0\left(\frac{1}{2}\mathrm{e}^{-(x_0-\alpha')^2} + x_0\frac{\sqrt{\pi}}{2}\mathrm{erfc}(x_0-\alpha')\right). \tag{27}$$

We simplify the final integration using $\xi \equiv x_0 - \alpha'$, so that

$$0 = \int_0^{\infty}\mathrm{d}\xi\left(\mathrm{e}^{-\xi^2} + \xi\sqrt{\pi}\mathrm{erfc}(\xi) + \alpha'\sqrt{\pi}\mathrm{erfc}(\xi)\right), \tag{28}$$

from which it follows that

$$\alpha' = \frac{\frac{1}{2} - \int_0^\infty \mathrm{d}\xi\,\xi\,\mathrm{erfc}(\xi)}{\int_0^\infty \mathrm{d}\xi\,\mathrm{erfc}(\xi)} = \frac{\sqrt{\pi}}{4}. \tag{29}$$

Returning to the units of length used in the main body of the text, we find $\alpha = 2\alpha' = \sqrt{\pi}/2 \simeq 0.89$. Hence, we see that using the approximation of a uniform $\rho(x_0)$, a result within 7% of the empirically found value can be obtained.